THE JOURNAL OF PHYSICAL CHEMISTRY C

pubs.acs.org/JPCC Article

Third- and Fifth-Order Nonlinear Optical Response of a TICT/Stilbene Hybrid Chromophore

Alexander J.-T. Lou,[‖] Sepehr Benis,[‖] Munan Gao, Alexander Baev, David Kim, Eric W. Van Stryland, David J. Hagan, and Tobin J. Marks*

Cite This: https://dx.doi.org/10.1021/acs.jpcc.9b11735 Read Online

ACCESS | Metrics & More | Article Recommendations | Supporting Information

ABSTRACT: Twisted intramolecular charge transfer (TICT) chromophores exhibit a promising third-order nonlinear optical (NLO) response, γ, which is potentially useful for all-optical switching. Here we explore the third- and fifth-order NLO response of a newly synthesized chromophore, **TMC-3′**, which incorporates both stilbene and TICT motifs with optical function. Solution *Z*-scan measurements in CH_2Cl_2 reveal modest two-photon absorptions (2PA) at 1100 and 800 nm (σ_{2PA} > 80 GM), and two contributions to the nonlinear refraction. The first component is attributed to the third-order bound-electronic response, while the second is assigned to a fifth-order process involving 2PA induced excited state refraction (2PA-ESR). Quantum computation suggests that the differences between the present work and previous studies lie primarily in the addition of the stilbene related states, as well as the increase in ground state dipole moment. This work yields insight into the third- and fifth-order NLO response of TICT chromophores and demonstrates that subtle structural modifications significantly impact their functionality.

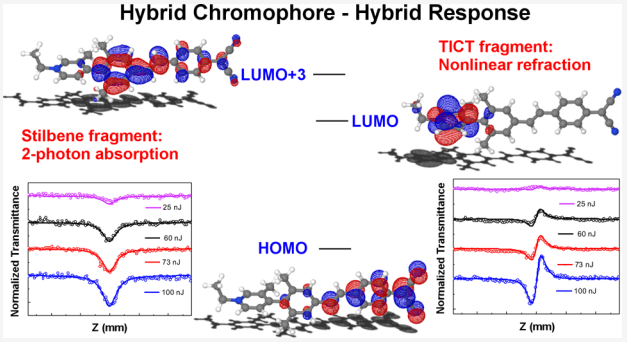

INTRODUCTION

Materials that exhibit nonlinear refraction (NLR) and absorption (NLA) have drawn significant interest for their applications in all-optical signal processing and optical power limiting, respectively.[1−6] The most commonly reported mechanism of NLR arises from the direct third-order nonlinearity, which occurs on a very short time scale (i.e., instantaneous NLR),[7] and manifests in bulk materials as the bound-electronic nonlinear refractive index n_2. In molecular materials this property is related to the second hyperpolarizability, γ, of the constituent chromophores. Strategies to enhance γ include bond length alternation (BLA), which involves balancing neutral and charged contributions to the ground state, creation of 2-D chromophores,[8,9] inclusion of auxiliary heterocyclic donor moieties, and optimization of the chromophore environment.[10−18] Our previous work has focused on the design of twisted intramolecular charge transfer (TICT) chromophores which feature a donor and acceptor fragment connected by a twisted biaryl bridge. The degree of biaryl torsion leads to localization of the HOMO and LUMO on the donor and acceptor fragment respectively, which results in a very large ground state dipole moment (μ_g), low charge transfer energy (E_{ge}), and a modest CT transition dipole (μ_{ge}).[19−21] Several modifications of the archetypal chromophore **TMC-2** (Figure 1), such as donor and acceptor group modification ($\mathbf{PMe_3TC_6(CN)_2}$) and coupling to a cyanine dye (**Cy-TICT**), lead to enhanced experimental γ values.[15,19,22]

Higher order processes have also been found to contribute to NLR and NLA in inorganic semiconductors and organic chromophores.[23−27] This contribution arises via a sequential, effectively fifth-order nonlinear process, in which two-photon absorption (2PA) is followed by excited state absorption and/or refraction.[24,28] Such processes can be denoted by $\chi^{(3)}$:$\chi^{(1)}$. For the case of an irradiance-dependent NLR, this is quantified on the molecular scale by an excited state refraction (ESR) cross-section (σ_{ESR}) and 2PA cross-section δ_{2PA}, which is related to the 2PA absorption coefficient, α_2, via $\delta_{2PA=}\frac{\hbar\omega}{N}\alpha_2$, where ω is the laser frequency and N is the total molecular density. The initial 2PA process is a relatively common phenomenon in organic chromophores and the design principles are now well understood for several structure types.[6] σ_{ESR} can in principle be observed in any molecule for which population is created via linear loss or nonlinear absorption (e.g., 2PA), and the ground and excited state

Received: December 20, 2019
Revised: February 3, 2020
Published: February 6, 2020

https://dx.doi.org/10.1021/acs.jpcc.9b11735
J. Phys. Chem. C XXXX, XXX, XXX−XXX

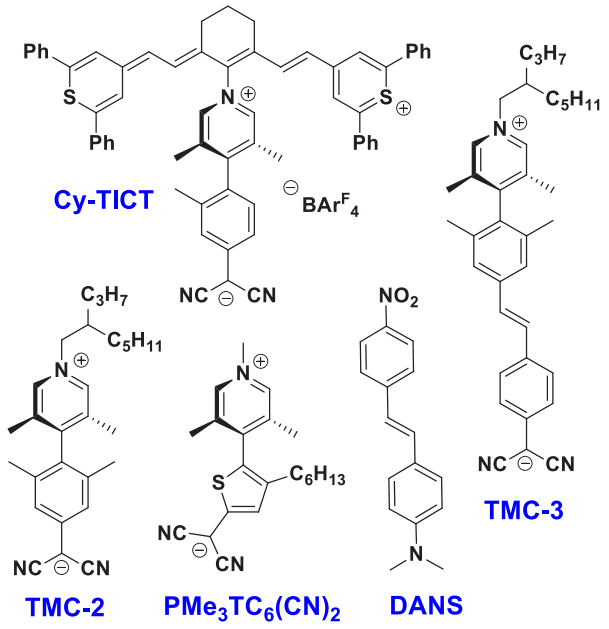

Figure 1. Archetypal TICT chromophore **TMC-2**, thiophene derivative $\mathbf{PMe_3TC_6(CN)_2}$, TICT/stilbene chromophore **TMC-3**, and cyanine/TICT hybrid **Cy-TICT**.

polarizability differs, although literature reports of σ_{ESR} and its contribution to NLR are somewhat scarce.[23−26,29]

In this study, we investigate the impact of appending a stilbene fragment to archetypal chromophore **TMC-2,** to form **TMC-3′**. In the past, this modification greatly enhanced second-order NLO response in the closely related **TMC-3** chromophore, primarily due to the increase in ground state dipole moment.[30,31] Here, we perform *Z*-scan measurements on **TMC-3′** at multiple irradiances and wavelengths in order to ascertain, (1) the 2PA cross-section (δ_{2PA}); (2) the second hyperpolarizability (γ); (3) the presence and dispersion of σ_{ESR} induced by 2PA. In order to understand the experimental results, we pursue electronic structure calculations to investigate the impact of molecular torsion, π-system elongation, and states residing on the stilbene fragment which are unique to this TICT system.

EXPERIMENTAL METHODS

Nonlinear Optical Characterization by *Z*-scan. The third- and fifth-order nonlinear optical response of **TMC-3′** was measured by the *Z*-scan method, which probes the change in absorption and refraction of a sample as a function of local light irradiance.[32] This experiment operates in two modes referred to as open aperture (OA), which reveals the NLA, and closed aperture (CA) used to determine NLR. The CA divided by OA (i.e., CA/OA) will decouple the NLR and NLA. In this investigation, we used a dual-arm *Z*-scan (DA *Z*-scan) setup, which allows for measurement of the solute by subtracting the solvent signal while directly accounting for beam fluctuations.[33] DA *Z*-scan can increase the signal-to-noise ratio (SNR) by an order of magnitude compared to single arm *Z*-scan in both solution and thin-film samples.[33,34] In order to determine both the dispersion and origin of NLA and NLR, measurements were performed using several irradiances at 800, 1100, and 1300 nm. **TMC-3′** solutions were prepared in dry CH_2Cl_2 at ∼1 mM concentration. Further details of nonlinear optical measurements are presented in Section S2 of the Supporting Information.

Computational Methods and Polarizability Calculations. Model **TMC-3′** analogues were optimized in the gas phase and with a polarizable continuum model for CH_2Cl_2 at the B3LYP/6-31G** level. The optimized torsional angles of ∼90° in CH_2Cl_2 are in good agreement with previous work and crystallographic data.[19,30,35] Molecular second hyperpolarizability, γ, was calculated in the Amsterdam density functional package using CAM-B3LYP/6-31+G*.[36] TDDFT was performed in Q-Chem using CAM-B3LYP/6-31+G** on **TMC-3′** structures with constrained biaryl dihedral angles of 65°, 70°, 75°, 80°, 85°, 89°.[37] Calculation of polarizabilities (α) can be performed using expressions obtained from perturbation of a molecular dipole moment (μ) with an electric field (F) (eq 1). The finite field (FF) method involves the calculation of state dipole moments at

$$\mu(F) = \mu_0 + \alpha F + \frac{1}{2}\beta F^2 + \cdots \quad (1)$$

applied static fields, fitting the results with eq 1. This method does not provide information about the relative contribution of specific states, nor does it account for the frequency dependence of polarizability, but allows qualitative comparisons without requiring knowledge of higher excited-state

Scheme 1. Synthesis of Chromophore TMC-3′[a]

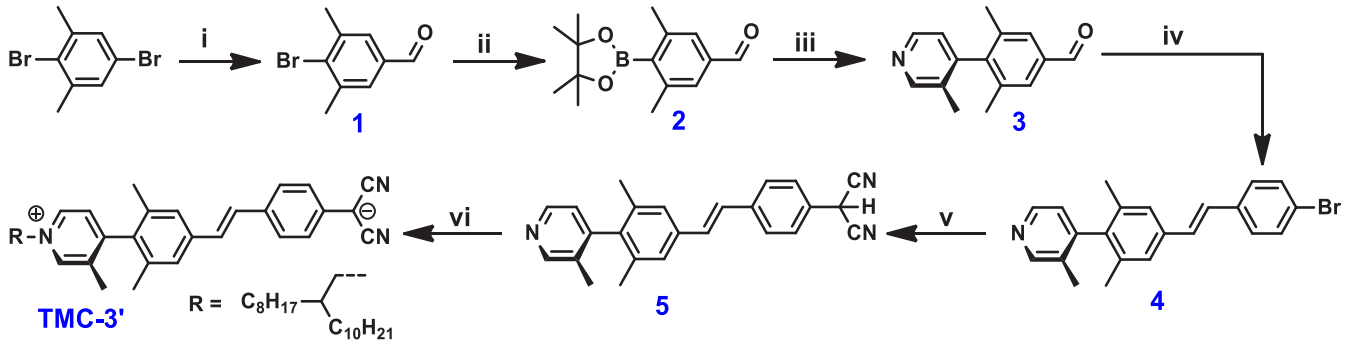

[a]Reaction conditions: (i) (a) *n*-BuLi, −78 °C, THF; (b) DMF; (ii) $Pd(PPh_3)_2Cl_2$, B_2pin_2, KOAc, 1,4-dioxane; (iii) 4-bromopyridine·HCl, $Pd_2(dba)_3$/SPhos, K_3PO_4, toluene/water; (iv) diethylbromobenzylphosphonate, KOtBu, THF; (v) $NaCH(CN)_2$, $Pd(PPh_3)_4$, NaH, DME; (vi) ROTf in CH_2Cl_2 and then NaOMe in MeOH.

https://dx.doi.org/10.1021/acs.jpcc.9b11735
J. Phys. Chem. C XXXX, XXX, XXX−XXX

characteristics, which are often unreliable.[38−41] The sum-over-states (SOS) method (eq 2) provides a complementary approach by directly correlating α with the characteristics of specific states; the full expression for α of state n is given by eq 2. Here n and m represent

$$\alpha_n(\omega) = \sum_{n \neq m} \left[\frac{\langle \psi_m | \hat{\mu} | \psi_n \rangle^2}{E_{nm} - \hbar\omega} \right] \quad (2)$$

different electronic states, μ is the transition moment between states, and E_{nm} is the difference in state energy.

In this work, we employ the SOS approach to calculate α from experimental data, and the FF method to obtain static α for ground and excited states by computing ground and excited-state dipole moments in the presence of static fields ranging from −0.001 to +0.001 au in 0.0001 au increments. Small fields were used both to limit the contribution of higher-order terms and to prevent reordering of the relevant states, which are somewhat closely spaced. Even so, careful interpretation of the state dipoles was required to obtain accurate results (see Supporting Information). The results were fit with the Taylor (or polynomial) method, including the hyperpolarizability (β) term for accuracy.

RESULTS AND DISCUSSION

Chromophore Design and Synthesis. Based on crystallographic and computational evidence, we have employed a tri-*o*-methyl biaryl fragment to provide a twist-inducing steric effect comparable to that of the more synthetically tedious tetra-*o*-methyl moiety.[35] The synthesis (Scheme 1) begins with conversion of 2,5-dibromo-1,3-dimethylbenzene to **1** via regioselective lithiation followed by treatment with dimethylformamide. The aryl bromide **1** is catalytically converted to **2**, which is then coupled to 4-chloro-3-methylpyridine·HCl using Suzuki coupling. Intermediate **3** is then converted to **4** by an *E*-selective Horner−Wadsworth−Emmons reaction with diethyl-4-bromo-benzylphosphonate. Pd-catalyzed coupling of **4** to malononitrile, subsequent alkylation with 2-octyldecyl triflate, and treatment with base affords **TMC-3′** in an overall yield of 32% over six steps. The product and key intermediates were characterized by ^{1}H NMR, ^{13}C NMR, elemental analysis, and mass spectrometry (see Supporting Information for more details). The inclusion of a bulky alkyl group renders **TMC-3′** sufficiently soluble to make the highly concentrated solutions needed for NLO characterization.

Vibrational Spectroscopy. The strength and frequency of CN stretching modes, ν(CN), are diagnostic of the electron density located on the dicyanomethanide group. Here we observe ν(CN) = 2162 cm^{-1} and a low energy side component at 2112 cm^{-1} in the solid state (Figure S3). Similar bands of 2164 and 2118 cm^{-1} are found in **TMC-3**, and the quantitative agreement of ν(CN) to that of a phenylmalononitrile carbanion (ν(CN) = 2163, 2117 cm^{-1}) suggests that the dicyanomethanide fragment in **TMC-3′** supports nearly a full negative charge, consistent with a zwitterionic ground state.[30,42]

Linear Optical Absorbance Spectroscopy of TMC-3′. The linear optical absorption of **TMC-3′** in CH_2Cl_2 (Figure 2A) is characterized by an intense subfragment charge transfer (SFCT) at 425 nm (ε = 32 000 M^{-1} cm^{-1}) and a weaker interfragment charge transfer (ICT) band at 542 nm (ε = 2130 M^{-1} cm^{-1}). The two low-energy excitations highlight the

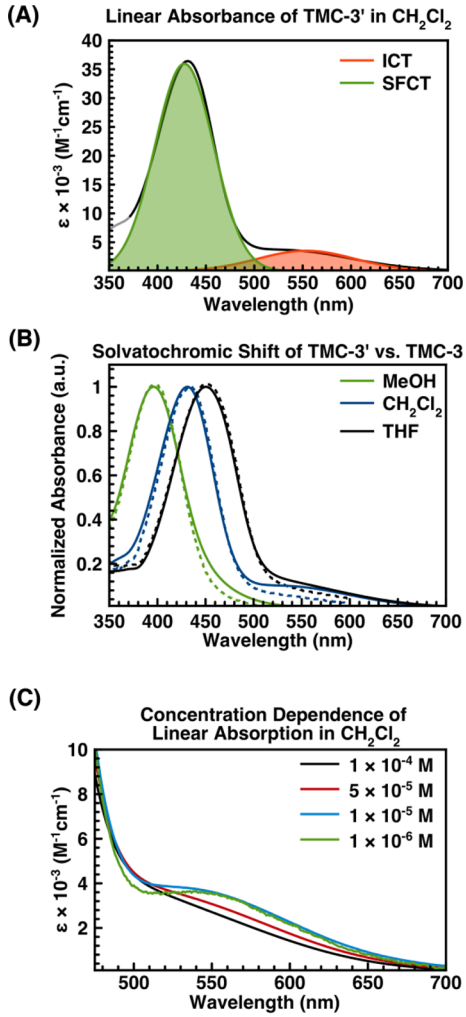

Figure 2. (A) Fitting of ICT and SFCT peaks of **TMC-3′** (~10^{-5} M) in CH_2Cl_2 (B) Comparison of solvatochromic shift of **TMC-3′** (solid lines) and **TMC-3** (dotted lines). (C) Concentration dependent absorption of **TMC-3′** in CH_2Cl_2, focused on the ICT peak.

hybrid nature of **TMC-3′**; the ICT excitation is similar in energy and strength (μ_{01} = 2.3 D) to that of **TMC-2** (560 nm in CH_2Cl_2), while the SFCT excitation has a large transition moment (μ_{02} = 8.3 D) typical of a donor/acceptor stilbene.[6,43] Comparison of the change in ICT ($\Delta\lambda \sim -77$ nm) and SFCT ($\Delta\lambda = -32$ nm) peak maxima in CH_2Cl_2 and MeOH solutions suggest that the magnitude of the state dipole moments increases in the order of $\mu_{ICT} < \mu_{SFCT} < \mu_g$. The linear absorbance characteristics of **TMC-3′** are nearly identical to those of previously reported **TMC-3**, which exhibits ICT and SFCT strengths of 2040 and 38 400 M^{-1} cm^{-1} respectively, and an equivalent solvatochromic shift of the SFCT peak (Figure 2B).[35]

As was previously identified by NMR experiments on **TMC-3**, the large μ_g of these chromophores creates a tendency toward aggregate formation, even in relatively dilute solutions.[30,35] The hypsochromic shift of the ICT band with increasing concentration in CH_2Cl_2 (Figure 2C) confirms a similar tendency, and it is therefore expected that highly concentrated solutions (>10^{-3} M) used for *Z*-scan measurements contain a non-negligible population of aggregates.

TICT/Stilbene Hybrid Molecular Orbitals. Molecular orbital pictures provide a useful qualitative view of the three

https://dx.doi.org/10.1021/acs.jpcc.9b11735
J. Phys. Chem. C XXXX, XXX, XXX−XXX

relevant orbitals: (1) the HOMO, which is mainly localized on the donor fragment and has little to no electron density on the acceptor side of the twisted bridge; (2) the LUMO, which mainly resides on the pyridinium ring with a small amount of electron density on the twisted bridge; (3) the LUMO+3 orbital, which resides primarily on the central region of the molecule. Note that relaxation of the biaryl twist angle can lead to delocalization of LUMO+3 onto the acceptor fragment (Figure 3). This qualitative picture highlights the unique

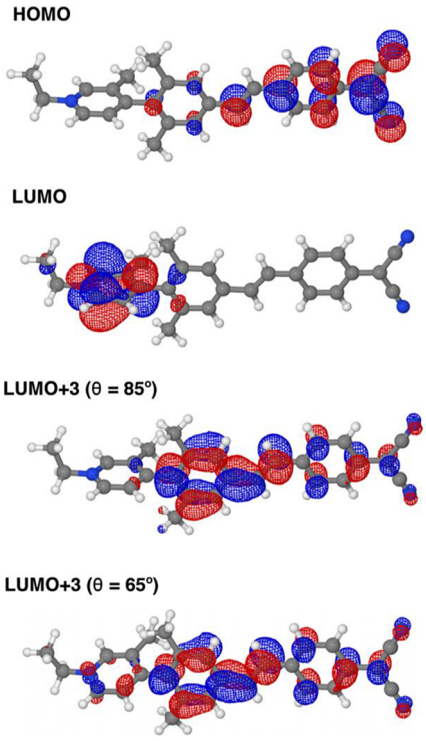

Figure 3. MO pictures of **TMC-3′** (85°) calculated at the CAM-B3LYP/6-31+G** level, cutoff set to 0.03.

character of the **TMC-3′** chromophore. Planar stilbenes are typically uniformly conjugated such that the HOMO and LUMO are both relatively delocalized over large portions of the π-system.[44] In contrast, **TMC-3′** has a segmented electronic structure reflecting the twisted biaryl fragment, and leading to HOMO and LUMO localization. The ICT and SFCT transitions have HOMO → LUMO and HOMO → LUMO+3 character, respectively.

NLO Characterization by *Z*-scan Measurements. OA measurements were performed at different pulse irradiances and wavelengths. The linear scaling of the signal versus pulse irradiance indicates 2PA is the dominant mechanism in NLA at each wavelength, as evidenced by satisfactory fitting of experimental data with a 2PA model, in agreement with the linear optical spectra, and computational results. OA measurements (Figure S1) reveal a small 2PA cross section of $\delta_{2PA} < 7$ GM at 1300 nm, and larger values of 110 ± 10 and 90 ± 10 GM at 800 and 1100 nm respectively (Table 1, Figures 4A and S1). δ_{2PA} at 800 nm is the highest measured value, consistent with the proximity to a two-photon (2P) resonance of the strongly absorbing SFCT state, and is similar to that of donor/acceptor stilbene molecules, such as DANS (~200 GM maximum in CH_2Cl_2).[42,43] δ_{2PA} at 1100 nm is also appreciable, likely enhanced by proximity to the ICT 2P resonance. These values exceed that of TICT chromophores **TMC-2** (8.9 GM at 800 nm) and **$PMe_3TC_6(CN)_2$**,[15,19] but are significantly smaller than the best known two-photon absorbers (>10000 GM).[6]

CA/OA measurements (Figure S1) reveal that the magnitude of the NLR response depends quadratically on the irradiance of the input beam, indicating the presence of a higher-order nonlinearity (Figure 4C). The fit to the *Z*-scan signals were performed by considering the analytical expression for the instantaneous NLR and excited-state nonlinearities as explained in Said et al.[24,45] In addition, the contribution of the instantaneous bound-electronic NLR, γ, was obtained from the intercept of the fitted line to the irradiance dependence of the CA/OA normalized transmittance (Figure 4C), and the ESR cross-section is found from the slope (see Section S2 for details). These values are in a good agreement with the analytical fits.[24,45] The irradiance-independent response ($\mathrm{Re}(\gamma) = -110 \pm 20 \times 10^{-35}$ esu) at 1100 nm exceeds that of **TMC-2**, but is relatively small at 800 and 1300 nm. We note that the value of the ESR cross-section at 1300 nm is a lower limit. This approximation is based on the upper limit that is reported for the 2PA at this wavelength.

Based on the observed 2PA, we conclude that the underlying dominant mechanism for irradiance-dependent NLR is sequential 2PA-ESR. In general, linear absorption (i.e., $\chi^{(1)}$) can also contribute to promoting carriers into the excited state, however, at these wavelengths the linear absorption is near zero. Therefore, our model only includes pure third-order nonlinear effects, i.e., $\chi^{(3)}$, and effective fifth-order nonlinear effects, i.e., $\mathrm{Im}\chi^{(3)}$:$\mathrm{Re}\chi^{(1)}$. This model explains the linear dependence of the measured NLR with the peak irradiance, which is discussed later in more detail. The values for γ and σ_{ESR} calculated directly from NLR and NLA values extracted

Table 1. Comparison of TMC-3′ and TMC-2 *Z*-Scan Results in CH_2Cl_2[a]

	TMC-3′			TMC-2[b]	
	800 nm	1100 nm	1300 nm	~775 nm	~1170 nm
$\mathrm{Re}(\gamma)$ (GM)	−5.0 ± 1	−70 ± 15	<2 ± 1	–	–
$\mathrm{Re}(\gamma)$ ($\times 10^{-35}$ esu)	−4.0 ± 1	−110 ± 20	<4 ± 2	140	50
σ_{ESR} ($\times 10^{-16}$ cm^2)	3.0 ± 0.5	5.5 ± 1	>13 ± 2	–	–
δ_{2PA} (GM)	110 ± 10	90 ± 10	<7.0	8.9	<1.5
δ_{2PA} ($\times 10^{-35}$ esu)	45 ± 5	70 ± 10	<7.5	–	–
linear transmittance	~0.99	~0.99	~0.99	~0.98	~0.99

[a]Here, $\mathrm{Re}(\gamma)$ is the 2nd hyperpolarizability related to the electronic nonlinear refraction, σ_{ESR} is the fifth-order nonlinear refraction due to the generated excited states via 2PA. δ_{2PA} is the 2PA absorption cross-section. The linear transmittance does not include losses from the Fresnel reflection. [b]Data from ref 19.

https://dx.doi.org/10.1021/acs.jpcc.9b11735
J. Phys. Chem. C XXXX, XXX, XXX−XXX

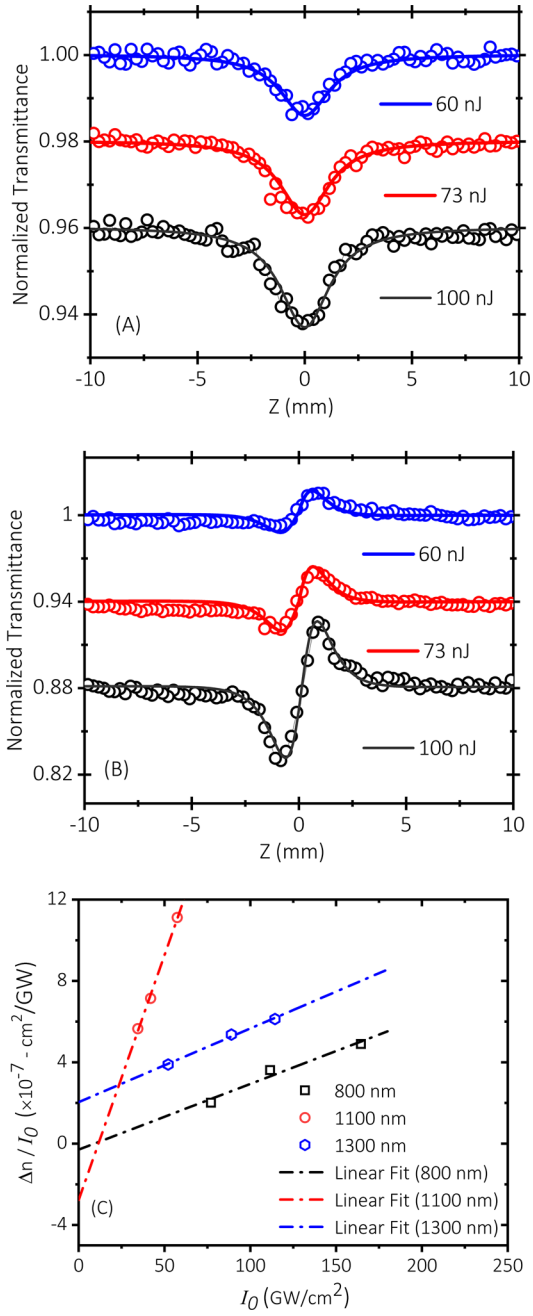

Figure 4. (A) OA *Z*-scan results for **TMC-3′** in CH_2Cl_2 at 1100 nm with 2PA fitting. (B) CA/OA results at 1100 nm fit for the second hyperpolarizability and 2PA-ESR. (C) Total nonlinear refraction divided by the peak input irradiance, I_0, versus the irradiance for three different wavelengths, indicating that the mechanism for NLR is a sequential 5th-order process involving 2PA created excited states followed by ESR. (*Z*-scan results for 800 and 1300 nm are reported in Section S2).

from the *Z*-scan, are reported in Table 1 in two different units, and the observed trends are discussed below.[46]

Computation of NLA and Excited State Character. Quantum computation reveals a maximum δ_{2PA} of 841 GM at ~1000 nm, which results from 2P excitation to the LUMO+3 orbital (Figure 3), which resides on the central and donor ring. Note that the computational value is calculated at 2P resonance, while the measured value at 800 nm is detuned from the 2P resonance, accounting partially for the discrepancy in magnitude. The transition from HOMO to LUMO+3 resembles CT which occurs in donor/acceptor stilbenes, suggesting that the central ring in **TMC-3′** functions as an auxiliary acceptor group. Accordingly, the strength and energy of this transition is comparable to simple donor/acceptor stilbenes.[43,44,47]

Computation of Third Order NLR. Calculations of Re(γ) were performed at wavelengths ranging from 775 to 1500 nm in order to encompass the technologically relevant window and to include regions of one- and two-photon enhancement (Table 2). Model compound **TMC-3′-EH** (see Section S3)

Table 2. Dispersion of Average Second Hyperpolarizability of TMC-3′-EH and TMC-2 Computed with CAM-B3LYP/6-31+G**

wavelength (nm)	TMC-3′-EH (10^{-35} esu)	TMC-2 (10^{-35} esu)
775	−680	~50378
900	−901	–
1000	10037	4735
1305	251	67
1550	166	15
inf	100	0.5

shows a change in sign of Re(γ) around 900−1000 nm. This corresponds to the region of the 2P resonance of the ICT state, indicating that the observed nonlinearity is dominated by the ICT contribution rather than the SFCT one. This is in agreement with the experimental data, which shows enhanced Re(γ) at 1100 nm, near the ICT 2P resonance. The difference in sign is a result of the discrepancy between computed and measured ICT energy, as the sign of Re(γ) changes upon crossing the 2P resonance. Note that it is not practical to directly compare computational and experimental values, as they may differ for a variety of reasons, including the overestimation of CT energy resulting from DFT pathologies, artificially high computed resonant enhancement, and solvent and aggregation effects. However, comparison between the two computed data sets provides valuable insight. Computed Re(γ) is uniformly larger for **TMC-3′-EH** than for **TMC-2**, with the exception of ~775 nm where **TMC-2** benefits from significant one-photon enhancement. At the static limit, Re(γ) of **TMC-3′-EH** (Figure 1) is 2 orders of magnitude larger than that of **TMC-2**.[19]

The static results (last entry in Table 2) can be understood in the context of a static 3-state description (eq 3) of Re(γ), where μ_{0n} is the transition moment between states 0 and *n*, E_{0n} is the energy gap, and $\Delta\mu_{0n}$ is the change in state dipole moment.

$$\gamma = -\frac{{\mu_{01}}^4}{{E_{01}}^3} + \frac{{\Delta\mu_{01}}^2{\mu_{01}}^2}{{E_{01}}^3} + \frac{{\mu_{01}}^2{\mu_{12}}^2}{{E_{01}}^2 E_{02}} \quad (3)$$

As $\Delta\mu_{01} \gg \mu_{01}$ for TICT chromophores, the second (dipolar) term is the primary contributor to Re(γ). Thus, the computed increase in Re(γ) far from resonance is the result of the extended π-system length, which causes $\Delta\mu_{01}$ to increase by ~25 D relative to **TMC-2**. These values are ~8× lower than those computed at 1550 nm for thiophene-based TICT chromophore $\mathbf{PMe_3TC_6(CN)_2}$, likely as a result of the significantly compressed HOMO−LUMO energy gap in that molecule.[15]

https://dx.doi.org/10.1021/acs.jpcc.9b11735
J. Phys. Chem. C XXXX, XXX, XXX−XXX

Origins of Excited State Refraction. The generation of excited states of density N_{ex} is governed by the 2PA as $dN_{ex}/dt = \alpha_2 I^2/2\hbar\omega$, and the change in index from the creation of these excited states is $\Delta n_{ESR} = \sigma_{ESR} N_{ex}/k_0$, with the ESR cross section in units of cm^2. We note that sometimes the k_0 is omitted, giving the cross section in units of cm^3. Thus, the total change in the refractive index, Δn, can be described as

$$\Delta n \cong n_2 I_0 + \frac{\sigma_{ESR}}{k_0}\frac{\alpha_2}{2\hbar\omega}\int_{-\infty}^{t} I^2(t')\,dt' \tag{4}$$

In eq 4, ω is the frequency of the photon, n_2 is the bound-electronic NLR related to γ, and k_0 is the free-space wavevector. By simplifying this equation (discussed in Section S2), we plot Δn divided by the peak input irradiance, I_0, as a function of I_0. The complete derivation of this equation is presented in Section S2. The change in refractive index induced by changes in the populations of ground and excited state is related to the difference in ground (α_g) and excited state polarizability (eq S5). The full sum-over-states expression for α (eq 2) can be truncated to a three-state model (eq 5) and used to derive α_g from the lowest two excited states of **TMC-3′** obtained from linear absorbance spectra in CH_2Cl_2 (Figure 2A).

$$\alpha_g(\omega) \approx \mu_{01}{}^2\left[\frac{1}{E_{01}-\hbar\omega}+\frac{1}{E_{01}-\hbar\omega}\right] + \mu_{02}{}^2\left[\frac{1}{E_{02}-\hbar\omega}+\frac{1}{E_{02}-\hbar\omega}\right] \tag{5}$$

Here, E_{0m} and μ_{0m} are the difference in the energy between the two states 0 and m, and the transition dipole moment of the transition involved, respectively, and ω is the input frequency. Substitution into eq 5 reveals $\alpha_g(800\text{ nm}) = 2.99 \times 10^{-22}$, $\alpha_g(1100\text{ nm}) = 2.47 \times 10^{-22}$, $\alpha_g(1300\text{ nm}) = 2.35 \times 10^{-22}$ cm^3, $\alpha_g(\text{static}) = 2.09 \times 10^{-22}$ cm^3 (or esu), and that the strongest contribution to polarizability arises from the SFCT.

The finite field (FF) method, described in the Experimental Methods, computes a static $\alpha_g = 1.99 \times 10^{-22}$ cm^3 at $\theta = 89°$, which is in good agreement with the SOS value derived from the experimental spectra (Table S2), justifying the reliability of this method. FF calculations also show that the α_g and SFCT state polarizability (α_{sfct}) are similar at the static limit (Figure 5). Both exceed α_{ICT}, as expected from the greater delocalization in the HOMO and LUMO+3 orbitals. These calculations also reveal that α is highly sensitive to the torsional angle (θ) of the biaryl fragment (Figure 5), as seen in previous literature.[48] There is a sharp increase in α_{sfct} upon relaxation from 89° to 85°, concurrent with greater delocalization of the relevant orbitals (Figure 3, LUMO+3). Such relaxation of θ in the excited state would be feasible given the quinoidal character of the LUMO+3 orbital, although without knowing the precise structure of the excited state, it is not possible to reliably compute α_{sfct} or σ_{ESR}.[49,50] The FF method (Table 3) is also unable to account for the effects of resonant enhancement, which dictate the dispersion of α for a given state. Thus, while we have been able to draw conclusions far from resonance, it is difficult to predict even the ordering of α_g, α_{ICT}, and α_{SFCT} in the region relevant to our experimental results, and consequently, we cannot make any definitive statement as to the trend in σ_{ESR}. However, our analysis finds that while TICT chromophore NLO properties have generally been most strongly related to the donor and acceptor identity, the central ring is also important here as it impacts the LUMO+3, which in turn contributes to σ_{ESR}. Furthermore, it is clear that both ground and excited state torsional angles are important to NLO properties, whereas in the past only the ground state has been considered.

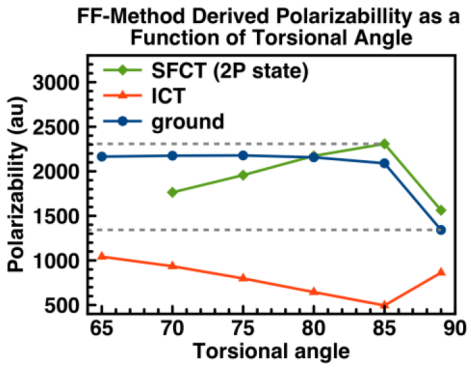

Figure 5. Computed static α of the ground, SFCT, and ICT states via the FF method, as a function of torsional angle (θ). Calculations were conducted using the ground state optimized geometry.

Table 3. Computed Dipole Moments and FF-Derived Polarizability and Hyperpolarizability of TMC-3′ at 85°

state	μ (D)[a]	α (10^{-22} esu)	β (10^{-33} esu)	σ_{ESR} (10^{-17} cm^2)
G	53.5	2.97	−7520	–
ICT	3.8	0.83	4620	−8.96
SFCT	34.0	3.48	−9540	2.13

[a]Computed via DFT.

CONCLUSIONS

We have investigated the third- and fifth-order nonlinear optical response of the hybrid TICT/stilbene chromophore, **TMC-3′**, finding that the orbitals centered primarily on the stilbene fragment lead to larger 2PA than observed in other TICT systems. In contrast to previous TICT results, there is a contribution from irradiance-dependent NLR, related to the change in polarizability between the ground and excited states. This work sheds new light on impact of molecular torsion in NLO chromophores, and it demonstrates that the addition of a stilbene fragment, while modestly enhancing Re(γ) at 1100 nm, also introduces linear and nonlinear effects which must be considered in the design of future chromophores.

ASSOCIATED CONTENT

Supporting Information

The Supporting Information is available free of charge on the ACS Publications Web site. The Supporting Information is available free of charge at https://pubs.acs.org/doi/10.1021/acs.jpcc.9b11735.

Details of quantum computation and experimental methods (PDF)

AUTHOR INFORMATION

Corresponding Author

Tobin J. Marks − *Department of Chemistry and the Materials Research Center, Northwestern University, Evanston, Illinois*

https://dx.doi.org/10.1021/acs.jpcc.9b11735
J. Phys. Chem. C XXXX, XXX, XXX−XXX

60208, United States; orcid.org/0000-0001-8771-0141; Email: t-marks@northwestern.edu

Authors

Alexander J.-T. Lou − *Department of Chemistry and the Materials Research Center, Northwestern University, Evanston, Illinois 60208, United States*

Sepehr Benis − *CREOL, College of Optics and Photonics, University of Central Florida, Orlando, Florida 32816, United States;* orcid.org/0000-0002-5442-7021

Munan Gao − *CREOL, College of Optics and Photonics, University of Central Florida, Orlando, Florida 32816, United States*

Alexander Baev − *The Institute for Lasers, Photonics and Biophotonics, State University of New York at Buffalo, Buffalo, New York 14260, United States*

David Kim − *Department of Chemistry and the Materials Research Center, Northwestern University, Evanston, Illinois 60208, United States*

Eric W. Van Stryland − *CREOL, College of Optics and Photonics and Department of Physics, University of Central Florida, Orlando, Florida 32816, United States*

David J. Hagan − *CREOL, College of Optics and Photonics and Department of Physics, University of Central Florida, Orlando, Florida 32816, United States;* orcid.org/0000-0003-2713-1767

Complete contact information is available at: https://pubs.acs.org/10.1021/acs.jpcc.9b11735

Author Contributions

‖These authors contributed equally

Notes

The authors declare no competing financial interest.

■ ACKNOWLEDGMENTS

We thank AFOSR Grant FA9550_12_1_0119 and MURI Grant FA9550_14_1_0040 for support of this research. A.J.-T.L. thanks the NDSEG for a graduate research fellowship. S.B, M.G, E.W.V.S, and D.J.H thank the Army Research Lab (W911NF-15-2-0090) for support.

■ REFERENCES

(1) Nozaki, K.; Tanabe, T.; Shinya, A.; Matsuo, S.; Sato, T.; Taniyama, H.; Notomi, M. Sub-Femtojoule All-Optical Switching Using a Photonic-Crystal Nanocavity. *Nat. Photonics* **2010**, *4*, 477−483.

(2) Hales, J. M.; Barlow, S.; Kim, H.; Mukhopadhyay, S.; Brédas, J.-L.; Perry, J. W.; Marder, S. R. Design of Organic Chromophores for All-Optical Signal Processing Applications. *Chem. Mater.* **2014**, *26*, 549−560.

(3) Bredas, J. L.; Adant, C.; Tackx, P.; Persoons, A.; Pierce, B. M. Third-Order Nonlinear Optical Response in Organic Materials: Theoretical and Experimental Aspects. *Chem. Rev.* **1994**, *94*, 243−278.

(4) Gubler, U.; Bosshard, C. Molecular Design for Third-Order Nonlinear Optics. *Adv. Polym. Sci.* **2002**, *158*, 123−187.

(5) Marder, S. R. Organic Nonlinear Optical Materials: Where We Have Been and Where We are Going. *Chem. Commun.* **2006**, 131−134.

(6) Pawlicki, M.; Collins, H. A.; Denning, R. G.; Anderson, H. L. Two-Photon Absorption and the Design of Two-Photon Dyes. *Angew. Chem., Int. Ed.* **2009**, *48*, 3244−3266.

(7) Gieseking, R. L.; Mukhopadhyay, S.; Risko, C.; Marder, S. R.; Bredas, J. L. 25th Anniversary Article: Design of Polymethine Dyes for All-Optical Switching Applications: Guidance from Theoretical and Computational Studies. *Adv. Mater.* **2014**, *26*, 68−83.

(8) Tykwinski, R. R.; Gubler, U.; Martin, R.; Diederich, F.; Bosshard, C.; Gunter, P. Structure-Property Relationships in Third-Order Nonlinear Optical Chromophores. *J. Phys. Chem. B* **1998**, *102*, 4451.

(9) Greve, D.; Schougaard, S. B.; Geisler, T.; Petersen, J. C.; Biornholm, T. Large Third-Order Nonlinear Optical Response from Molecuels with Effective Multidirectional Charge-Transfer Transitions: New Design of Third-Order Nonlinear Chromophores. *Adv. Mater.* **1997**, *9*, 1113−1116.

(10) Meyers, F.; Marder, S. R.; Pierce, B. M.; Bredas, J. L. Electric Field Modulated Nonliear Optical Properties of Donor-Acceptor Polyenes: Sum-Over-States Investigation of the Relationship between Molecular Polarizabilities (α, β, γ) and Bond Length Alternation. *J. Am. Chem. Soc.* **1994**, *116*, 10703−10714.

(11) Concilio, S.; Biaggio, I.; Gunter, P.; Piotto, S. P.; Edelmann, M. J.; Raimundo, J.-M.; Diederich, F. Third-Order Nonlinear Optical Properties of In-backbone Substituted Oligo(triacetylene) Chromophores. *J. Opt. Soc. Am. B* **2003**, *20*, 1656−1660.

(12) Hu, H.; Ensley, T. R.; Reichert, M.; Ferdinandus, M. R.; Peceli, D.; Przhonska, O. V.; Marder, S. R.; Jen, A. K.- Y.; Hales, J. M.; Perry, J. W.; Hagan, D. J.; Van Stryland, E. W.; et al. Optimization of the Electronic Third-Order Nonlinearity of Cyanine-Like Molecules for All Optical Switching. *Proc. SPIE* **2014**, *8983*, 898303.

(13) Gu, B.; Zhao, C.; Baev, A.; Yong, K.-T.; Wen, S.; Prasad, P. N. Molecular Nonlinear Optics: Recent Advances and Applications. *Adv. Opt. Photonics* **2016**, *8*, 328−369.

(14) Barlow, S.; Brédas, J.-L.; Getmanenko, Y. A.; Gieseking, R. L.; Hales, J. M.; Kim, H.; Marder, S. R.; Perry, J. W.; Risko, C.; Zhang, Y. Polymethine Materials with Solid-State Third-Order Optical Susceptibilities Suitable for All-Optical Signal-Processing Applications. *Mater. Horiz.* **2014**, *1*, 577−581.

(15) Teran, N. B.; He, G. S.; Baev, A.; Shi, Y.; Swihart, M. T.; Prasad, P. N.; Marks, T. J.; Reynolds, J. R. Twisted Thiophene-Based Chromophores with Enhanced Intramolecular Charge Transfer for Cooperative Amplification of Third-Order Optical Nonlinearity. *J. Am. Chem. Soc.* **2016**, *138*, 6975−6984.

(16) Kuzyk, M. G.; Singer, K. D.; Stegeman, G. I. Theory of Molecular Nonlinear Optics. *Adv. Opt. Photonics* **2013**, *5*, 4−82.

(17) Li, Z. a.; Kim, H.; Chi, S.-H.; Hales, J. M.; Jang, S.-H.; Perry, J. W.; Jen, A. K. Y. Effects of Counterions with Multiple Charges on the Linear and Nonlinear Optical Properties of Polymethine Salts. *Chem. Mater.* **2016**, *28*, 3115−3121.

(18) Matichak, J. D.; Hales, J. M.; Barlow, S.; Perry, J. W.; Marder, S. R. Dioxaborine- and Indole-Terminated Polymethines: Effects of Bridge Substitution on Absorption Spectra and Third-Order Polarizabilities. *J. Phys. Chem. A* **2011**, *115*, 2160−2168.

(19) He, G. S.; Zhu, J.; Baev, A.; Samoc, M.; Frattarelli, D. L.; Watanabe, N.; Facchetti, A.; Agren, H.; Marks, T. J.; Prasad, P. N. Twisted π-System Chromophores: Novel Pathway to All-Optical Switching. *J. Am. Chem. Soc.* **2011**, *133*, 6675−6680.

(20) Wang, Y.; Frattarelli, D. L.; Facchetti, A.; Cariati, E.; Tordin, E.; Ugo, R.; Zuccaccia, C.; Macchioni, A.; Wegener, S. L.; Stern, C. L.; Ratner, M. A.; Marks, T. J. Twisted π-Electron System Electrooptic Chromophores. Structural and Electronic Consequences of Relaxing Twist-Inducing Nonbonded Repulsions. *J. Phys. Chem. C* **2008**, *112*, 8005−8015.

(21) Albert, I. D. L.; Marks, T. J.; Ratner, M. A. Conformationally-Induced Geometric Electron Localization. Interrupted Conjugation, Very Large Hyperpolarizabilities, and Sizable Infrared Absorption in Simple Twisted Molecular Chromophores. *J. Am. Chem. Soc.* **1997**, *119*, 3155−3156.

(22) Shi, Y.; Lou, A. J.-T.; He, G. S.; Baev, A.; Swihart, M. T.; Prasad, P. N.; Marks, T. J. Cooperative Coupling of Cyanine and Tictoid Twisted π-Systems to Amplify Organic Chromophore Cubic Nonlinearities. *J. Am. Chem. Soc.* **2015**, *137*, 4622−4625.

(23) Said, A. A.; Sheik-Bahae, D. J.; Hagan, D. J.; Wei, T. H.; Wang, J.; Young, J.; Van Stryland, E. W. Determination of Bound-Electronic

and Free-Carrier Nonlinearities in ZnSe, GaAs, CdTe, and ZnTe. *J. Opt. Soc. Am. B* **1992**, *9*, 405−414.
(24) Said, A. A.; Wamsley, C.; Hagan, D. J.; Van Stryland, E. W.; Reinhardt, B. A.; Roderer, P.; Dillard, A. G. Third- and Fifth-Order Optical Nonlinearities in Organic Materials. *Chem. Phys. Lett.* **1994**, *228*, 646−650.
(25) Wang, C.; Fan, C.; Yuan, C.; Yang, G.; Li, X.; Ju, C.; Feng, Y.; Xu, J. Third- and High-Order Nonlinear Optical Properties of an Intramolecular Charge-Transfer Compound. *RSC Adv.* **2017**, *7*, 4825−4829.
(26) Zhan, C.; Zhang, D.; Zhu, D.; Wang, D.; Li, Y.; Li, D.; Lu, Z.; Zhao, L.; Nie, Y. Third- and Fifth-Order Optical Nonlinearities in a New Stilbazolium Derivative. *J. Opt. Soc. Am. B* **2002**, *19*, 369−375.
(27) Wei, T.; Hagan, D. J.; Sence, E.; Van Stryland, E. W.; Perry, J. W.; Coulter, D. Direct Measurement of Nonlinera Absorption and Refraction in Solutions of Phthalocyanines. *Appl. Phys. B: Lasers Opt.* **1992**, *54*, 46−51.
(28) Acioli, L. H.; Gomes, A. S. L.; Leite, J. R. R. Measurement of High-Order Optical Nonlinear Susceptibilities in Semiconductor-Doped Glasses. *Appl. Phys. Lett.* **1988**, *53*, 1788−1790.
(29) Zhan, C.; Xu, W.; Zhang, D.; Li, D.; Lu, Z.; Nie, Y.; Zhu, D. *Z*-scan Investigation of Fifth-Order Optical Nonlinearity Induced by Saturable-Absorption from (TBA)2Ni(dmit)2: Application for Optical Limiting. *J. Mater. Chem.* **2002**, *12*, 2945−2948.
(30) Kang, H.; Facchetti, A.; Jiang, H.; Cariati, E.; Righetto, S.; Ugo, R.; Zuccaccia, C.; Macchioni, A.; Stern, C. L.; Marks, T. J.; et al. Ultra-large Hyperpolarizability Twisted π-electron System Electro-Optic Chromophores. *J. Am. Chem. Soc.* **2007**, *129*, 3267−3286.
(31) Kang, H.; Facchetti, A.; Stern, C. L.; Rheingold, A. L.; Kassel, W. S.; Marks, T. J. Efficient Synthesis and Structural Characteristics of Zwitterionic Twisted π-electron System Biaryls. *Org. Lett.* **2005**, *7*, 3721−3724.
(32) Sheik-Bahae, M.; Said, A. A.; Wei, T. H.; Hagan, D. J.; Van Stryland, E. W. Sensetive Measurement of Optical Nonlinearities Using a Single Beam. *IEEE J. Quantum Electron.* **1990**, *26*, 760−769.
(33) Ferdinandus, M. R.; Reichert, M.; Ensley, T. R.; Hu, H.; Fishman, D. A.; Webster, S.; Hagan, D. J.; Van Stryland, E. W. Dual-Arm *Z*-scan Technique to Extract Dilute Solute Nonlinearities from Solution Measurements. *Opt. Mater. Express* **2012**, *2*, 1776−1790.
(34) Ensley, T. R.; Benis, S.; Hu, H.; Li, Z.; Jang, S. H.; Jen, A. K.; Perry, J. W.; Hales, J. M.; Hagan, D. J.; Van Stryland, E. W. Nonlinear Refraction and Absorption Measurements of Thin Films by the Dual-Arm *Z*-Scan Method. *Appl. Opt.* **2019**, *58*, D28−D33.
(35) Shi, Y.; Frattarelli, D.; Watanabe, N.; Facchetti, A.; Cariati, E.; Righetto, S.; Tordin, E.; Zuccaccia, C.; Macchioni, A.; Wegener.; et al. Ultra-High-Response, Multiply Twisted Electro-optic Chromophores: Influence of π-System Elongation and Interplanar Torsion on Hyperpolarizability. *J. Am. Chem. Soc.* **2015**, *137*, 12521−12538.
(36) Baerends, E. J. et al. *Amsterdam Density Functional, SCM*; Theoretical Chemistry, Vrije Universiteit: Amsterdam, The Netherlands.
(37) Shao, Y.; et al. Advances in Molecular Quantum Chemistry Contained in the Q-Chem 4 Program Package. *Mol. Phys.* **2015**, *113*, 184−215.
(38) Cai, Z.-L.; Sendt, K.; Reimers, J. R. Failure of Density-Functional Theory and Time-Dependent Density-Functional Theory for Large Extended π Systems. *J. Chem. Phys.* **2002**, *117*, 5543−5549.
(39) Furche, F.; Rappoport, D. Density Functional Methods for Excited States: Equilibrium Structure and Electronic Spectra. *Theor. Comput. Chem.* **2005**, *16*, 93−128.
(40) Maitra, N. T. Perspective: Fundamental Aspects of Time-Dependent Density Functional Theory. *J. Chem. Phys.* **2016**, *144*, 220901.
(41) Tozer, D. J.; Amos, R. D.; Handy, N. C.; Roos, B. O.; Serrano-Andres, L. Does Density Functional Theory Contribute to the Understanding of Excited States of Unsaturated Organic Compounds? *Mol. Phys.* **1999**, *97*, 859−868.
(42) Binev, Y. I.; Georgieva, M. K.; Novkova, S. I. The Conversion of Phenylpropanedinitrile (Phenylmalononitrile) into the Carbanion, Followed by IR Spectra, Ab Initio and DFT Force Field Calculations. *Spectrochim. Acta, Part A* **2003**, *59A*, 3041.
(43) Wicks, G.; Rebane, A.; Drobizhev, M. Two-Photon Solvatochromism of 4-dimethylamino-4'-nitrostilbene (DANS). *Proc. SPIE* **2014**, 89830R.
(44) Alam, M. M.; Chattopadhyaya, M.; Chakrabarti, S. On the Origin of Large Two-Photon Activity of DANS Molecule. *J. Phys. Chem. A* **2012**, *116*, 11034−11040.
(45) Said, A. A.; Sheik-Bahae, M.; Hagan, D. J.; Wei, T.; Wang, J.; Young, J.; Van Stryland, E. W. Determination of Bound and Free-Carrier Nonlinearities in ZnSe, GaAs, CdTe, and ZnTe. *J. Opt. Soc. Am. B* **1992**, *9*, 405−414.
(46) Ensley, T. R.; Hu, H.; Reichert, M.; Ferdinandus, M. R.; Peceli, D.; Hales, J. M.; Perry, J. W.; Li, Z. a.; Jang, S.-H.; Jen, A. K. Y.; et al. Quasi-Three-Level Model Applied to Measured Spectra of Nonlinear Absorption and Refraction in Organic Molecules. *J. Opt. Soc. Am. B* **2016**, *33*, 780−796.
(47) Krawczyk, P. DFT Study of Linear and Nonlinear Optical Properties of Donor-Acceptor Substituted Stilbenes, Azobenzenes and Benzilideneanilines. *J. Mol. Model.* **2010**, *16*, 659−668.
(48) Isborn, C. M.; Davidson, E. R.; Robinson, B. H. Ab Initio Diradical/Zwitterionic Polarizabilities and Hyperpolarizabilities in Twisted Double Bonds. *J. Phys. Chem. A* **2006**, *110*, 7189−7196.
(49) Grabowski, Z. R.; Rotkiewicz, K.; Rettig, W. Structural Changes Accompanying Intramolecular Electron Transfer: Focus on Twisted Intramolecular Charge-Transfer States and Structures. *Chem. Rev.* **2003**, *103*, 3899−4031.
(50) Maus, M.; Rettig, W. The Influence of Conformation and Energy Gaps on Optical Transition Moments in Donor-Acceptor Biphenyls. *Chem. Phys.* **2000**, *261*, 323−337.

https://dx.doi.org/10.1021/acs.jpcc.9b11735
J. Phys. Chem. C XXXX, XXX, XXX−XXX